Pergamon

*Int. J. Heat Mass Transfer.* Vol. 40, No. 5, pp. 1205–1216, 1997
Copyright © 1996 Elsevier Science Ltd
Printed in Great Britain. All rights reserved
0017–9310/97 $17.00+0.00

PII: S0017-9310(96)00081-6

# Theory of transient multicomponent transport coupling in three-dimensional stagnation flows

YORAM TAMBOUR†

Department of Mechanical and Aerospace Engineering Princeton University, Princeton, NJ 08544, U.S.A.

(*Received* 27 *June* 1994 *and in final form* 22 *September* 1995)

**Abstract**—A general field transformation for transient three-dimensional multicomponent energy and species equations is presented. Employing this transformation, transient multicomponent transport coupling effects in three-dimensional flows with surface injection cooling are studied. A new multicomponent transport coupling parameter is introduced and new results for the surface heat flux for various values (between 0 and 1) of this parameter are given. These values of the transport coupling parameter represent a wide range of transport properties of multicomponent mixtures. The present results demonstrate how a given final surface cooling efficiency can be obtained by choosing a variety of combinations of various values of the transport coupling parameter and injection rates. The present study also reveals an interesting behavior of local overshoot values in the transient relative contribution of the transport coupling effects to the surface heat flux. This behavior is explained here in terms of fluctuations in a multicomponent 'Transport-coupling Activity' number, which is sensitive to the differences in the characteristic rate of change of the local concentration gradients with respect to the local temperature gradient. Copyright © 1996 Elsevier Science Ltd.

## 1. INTRODUCTION

Transport-coupling phenomena have long been recognized as significantly affecting diffusion and heat fluxes in flow systems with large molecular weight disparities which are subject to concentration and temperature gradients [1–10]. Briefly, the term 'transport-coupling' refers to *thermal-diffusion* (or Soret effect) which is a diffusion flux due to a temperature gradient and *diffusion-thermo* (or Dufour effect) which is the transfer of heat due to concentration gradients.

In engineering devices in which surface mass transfer cooling is used as a method of obtaining tolerable surface temperatures, transport coupling effects may, under certain operating conditions (which depend on the relative magnitudes of the concentration and temperature gradients near the solid surfaces), cause considerable changes in the values of surface heat and mass fluxes. Such operating conditions have been studied intensively in the case of blowing light-molecular-weight gases into boundary layer flows [1, 4, 6, 7]. In these studies, a wide range of temperature differentials, free-stream concentrations, and surface blowing rates, usually in a binary (e.g. helium–air) system, have been analysed.

In other engineering applications which involve gas-phase or surface chemical reactions [11–17], transport-coupling effects may be enhanced via the steep temperature and concentration gradients formed as a result of these chemical reactions [14–17], and vice versa. For example, the opposite effect may occur in the case of diffusion-controlled surface chemical reactions, where the rate of diffusion may vary significantly due to thermal-diffusion and this affects the chemical reaction [16].

As to the mathematical treatment of these transport-coupling effects, a unique approach has been presented by Rosner [10] and by Srivastava and Rosner [9]. In this approach, the contributions of the transport-coupling effects to the diffusion and heat fluxes (and also contributions associated with variable properties) are treated as effective source and homogeneous chemical sink terms and are regarded as pseudo-blowing and pseudo-suction effects. Hence, the solutions and the analyses of the behavior of the flow systems which were considered in the above mentioned studies [9, 10], were based on analogies to the latter well-known effects.

Other mathematical approaches commonly used in the literature to study transport-coupling effects were discussed in detail by Taylor [8]. Generally, the extant studies are concerned with *steady-state* transport-coupling effects in *boundary-layer* type flows, e.g. see refs. [1, 4, 6, 7, 9, 10, 15–18], in which (i) gas-phase reactive, (ii) surface reactive and (iii) non-reactive boundary-layers were analysed.

Thus, in light of the above, it is the purpose of the present study to focus on *transient* transport-coupling effects in *general* 3D flow systems. An analysis of

† The author is currently on sabbatical leave from the Department of Aerospace Engineering, Technion-Israel Institute of Technology, Haifa 32000, Israel.

## NOMENCLATURE

$c_i$ mass fraction of species $i$, $(\rho_i/\rho)$
$c_{pi}$ specific heat of species $i$
$c_{pf}$ $\sum_i^n c_i c_{pi}$, specific heat at constant pressure
$D_{ij}$ multicomponent coefficient of diffusion of species $i$ due to concentration gradient of species $j$
$\bar{D}_{ij}$ equivalent multicomponent diffusion coefficient, equation (33)
$D_{iT}$ multicomponent thermal diffusion coefficient of species $i$
$\bar{D}_{iH}$ equivalent thermal-diffusion coefficient, equation (34)
$D_{Ti}$ multicomponent coefficient of diffusion-thermo due to concentration gradient of species $i$
$\bar{D}_j$ equivalent diffusion-thermo coefficient, equation (28)
$\hat{e}$ unit vector in the $e$ direction
$\dot{E}_K$ source term defined by equation (19)
$\dot{E}_T$ source term defined by equation (23)
$f_w$ wall injection parameter defined by equation (54)
$F$ general transport coupling parameter defined by equation (53)
$G$ function defined by equation (16)
$h$ enthalpy
$h^{(o)}$ enthalpy of formation
$h_e$ scale coefficient in the $e$ direction
$I$ $= h + \frac{1}{2}\mathbf{V}\cdot\mathbf{V}$, total energy
$\mathbf{J}_i$ mass flux of species $i$
$\mathbf{J}_q$ energy flux
$J$ Jacobian
$k$ coefficient of thermal conductivity
$\bar{k}$ equivalent thermal conductivity coefficient, equation (27)
$Le$ Lewis number
$\bar{Le}$ equivalent Lewis number, equation (30)
$\mathbf{M}$ modal matrix defined in the Appendix
$n$ number of species
$\bar{n}$ coordinate normal to surface
$p$ static pressure
$Pr$ Prandtl number
$\bar{Pr}$ equivalent Prandtl number, equation (29)
$\bar{Pr}_i$ equivalent 'Prandtl–Schmidt' numbers, equation (A1)
$r$ radial coordinate
$R$ radius
$Sc$ Schmidt number
$\bar{Sc}_{ij}$ equivalent diffusion Schmidt number, equation (35)
$\bar{Sc}_{iH}$ equivalent thermal-diffusion Schmidt number, equation (36)
$\dot{s}$ general source term
$\dot{\mathbf{S}}$ source term column vector defined by equation (40)
$t$ time
$T$ static absolute temperature
TA non-dimensional 'Transport-coupling Activity' number defined by equation (57)
$u$ velocity component parallel to surface
$u_i$ Cartesian velocity component
$U_\infty$ free stream velocity
$v$ velocity component normal to surface
$\mathbf{V}$ velocity vector
$w$ velocity component orthogonal to $u$ and $v$
$x$ coordinate along the surface
$y$ coordinate normal to the surface
$z$ coordinate orthogonal to $x$ and $y$.

Greek symbols

$\alpha_{ij}, \beta_j$ coupling coefficients
$\gamma_i, \gamma_{ji}$ coupling coefficients
$\Delta$ coefficient determinant, equation (A6)
$\delta_{ij}$ Kronecker delta
$\varepsilon$ zero for two-dimensional and unity for axisymmetric
$\zeta_j$ transformed 'total enthalpy-concentration field'
$\eta$ cooling efficiency defined by equation (55)
$\theta$ spherical coordinate
$\Theta$ function defined by equation (17)
$\kappa$ bulk viscosity
$\Lambda$ diagonal matrix with elements $\lambda_i$, defined in the Appendix
$\lambda_i$ eigenvalues of the matrix $\Omega$
$\mu$ viscosity
$\mu_{ij}$ elements of the inverse-modal matrix $\mathbf{M}^{-1}$
$\dot{\nu}_i$ rate of mass generation of species $i$ per unit volume due to chemical reactions
$\xi$ column vector defined by equation (24)
$\rho$ density
$\tau$ stress tensor
$\tau$ general non-dimensional time variable defined by equation (51)
$\tau_i$ non-dimensional time variable for each $\zeta_i$ field defined by equation (50)
$\Phi$ dissipation term
$\phi$ spherical coordinate
$\phi_i$ non-dimensional field variable defined by equation (49)
$\Omega$ transport coefficient matrix
$\omega$ row matrices equations (26), (32) and (38).

Subscripts

w wall
0 at the surface
$\infty$ free stream
$i,j$ chemical species
$\hat{i},\hat{j},\hat{k}$ in the Cartesian directions
q energy.

Superscripts

C transport coupling considered
NC transport coupling is *not* considered.

these transient effects may be of great importance for engineering applications such as rocket exhaust nozzles, re-entry vehicles, etc. in which it is desired to protect surfaces from high temperature gas streams at short operation time intervals. Transient transport-coupling effects may also be important in the analysis of the transport of heat and moisture in composite materials [20], and in treating droplet evaporation and spray combustion problems [21–26].

Generally, the relative contributions of transport-coupling effects to the heat and diffusion fluxes depend not only on the magnitude of the Soret (thermal-diffusion) and Dufour (diffusion-thermo) cross coupling coefficients, which are usually much smaller than the regular (Fourier's and Fick's) transport coefficients, but also on the *relative* magnitude of the local concentration gradients of the various species, with respect to the local temperature gradient. *Transient*-coupling effects however may, as will be shown in the present study, demonstrate unexpected behavior.

Specificaly, in *transient* systems one should be aware of the fact that the transient decay (or enhancement) of the initial temperature gradients may have a different characteristic time scale than the decay of the initial concentration gradients. Thus, an analysis of transient transport-coupling effects requires rigorous treatment, especially at short latencies as undertaken by the present study.

Thus, we begin (in Section 2) with the general three-dimensional (3D) non-steady field equations for a multicomponent compressible fluid, considering coupled transport fluxes. Then, in Section 3, a general field transformation is presented whereby the 3D energy and species equations are transformed into a widely useful 'energy-species' equation. This new 3D 'energy-species' field equation is employed in Section 4 for the analysis of transient multicomponent transport-coupling effects in 3D stagnation flows.

## 2. FLOW FIELD EQUATIONS AND COUPLED TRANSPORT FLUXES

The general 3D non-steady flow field equations for a multicomponent compessible fluid considering simultaneous heat and mass transfer can be written as:

Continuity:

$$\frac{\partial \rho}{\partial t} + \operatorname{div}(\rho \mathbf{V}) = 0 \tag{1}$$

Navier–Stokes equations:

$$\rho \frac{\mathrm{d}\mathbf{V}}{\mathrm{d}t} = -\operatorname{grad} p + \operatorname{Div} \boldsymbol{\tau} \tag{2}$$

Species:

$$\rho \frac{\mathrm{d}c_i}{\mathrm{d}t} = -\operatorname{div}(\mathbf{J}_i) + \dot{v}_i \quad i = 1,2,\ldots n-1 \tag{3}$$

Energy:

$$\rho \frac{\mathrm{d}h}{\mathrm{d}t} = \frac{\mathrm{d}p}{\mathrm{d}t} - \operatorname{div}(\mathbf{J}_q) + \Phi \tag{4}$$

where $\rho$ is the density, $t$ is the time, $\mathbf{V}$ is the velocity vector with Cartesian components $u_{\hat{i}}, u_{\hat{j}}, u_{\hat{k}}$ (or $u, v, w$) in the $x_{\hat{i}}, x_{\hat{j}}, x_{\hat{k}}$ (or $x, y, z$) directions, respectively; $p$ is the pressure, $c_i = \rho_i/\rho$ is the mass fraction of species $i$, $\mathbf{J}_i$ is the mass flux of species $i$, $\dot{v}_i$ is the rate of mass generation of the species $i$ per unit volume due to chemical reactions, $h$ is the specific enthalpy, $\mathbf{J}_q$ is the energy flux and $\Phi$ is the dissipation function; $\boldsymbol{\tau}$ is the stress tensor, which may (for a compressible Newtonian fluid) be described in a Cartesian-tensor notation as:

$$\tau_{\hat{i}\hat{j}} = \mu\left(\frac{\partial u_{\hat{i}}}{\partial x_{\hat{j}}} + \frac{\partial u_{\hat{j}}}{\partial x_{\hat{i}}} - \frac{2}{3}\frac{\partial u_{\hat{k}}}{\partial x_{\hat{k}}}\delta_{\hat{i}\hat{j}}\right) + \kappa \frac{\partial u_{\hat{k}}}{\partial x_{\hat{k}}}\delta_{\hat{i}\hat{j}} \tag{5}$$

where $\mu$ is the shear viscosity and the Kronecker delta $\delta_{\hat{i}\hat{j}}$ equals zero for $\hat{i} \neq \hat{j}$ and unity for $\hat{i} = \hat{j}$. The dissipation term $\Phi$ is given, in Cartesian coordinates, by

$$\Phi = \boldsymbol{\tau} : \operatorname{grad} \mathbf{V} = \mu \frac{\partial u_{\hat{i}}}{\partial x_{\hat{j}}}\left(\frac{\partial u_{\hat{j}}}{\partial x_{\hat{i}}} + \frac{\partial u_{\hat{k}}}{\partial x_{\hat{k}}}\right) - \left(\frac{2}{3}\mu - \kappa\right)\frac{\partial u_{\hat{k}}}{\partial x_{\hat{k}}}\frac{\partial u_{\hat{k}}}{\partial x_{\hat{k}}} \tag{6}$$

where $\kappa$, which appears in equations (5) and (6), is the bulk viscosity. It should be noted that the bulk viscosity terms, as well as the term $\dot{v}_i$ which describes the rate of formation of species $i$ due to chemical reactions, are given here only for the generality of the field transformation which will be presented in the next section. Bulk viscosity effects will not be analysed in the present study; a comprehensive study of these effects will be presented in a forthcoming paper [19]. As to chemical reactions, in the present study a non-reactive multicomponent system will be analysed.

The thermodynamically coupled diffusion and energy transport fluxes may be described by the phenomenological Linear Laws [15–18] as follows:

$$\mathbf{J}_i = -D_{ii} \operatorname{grad} c_i - \sum_{\substack{i=1 \\ i \neq j}}^{n-1} D_{ij} \operatorname{grad} c_j - D_{iT} \operatorname{grad} T \qquad i = 1,2,\ldots(n-1) \tag{7}$$

$$\mathbf{J}_q = -k \operatorname{grad} T - \sum_{i=1}^{n-1} D_{Ti} \operatorname{grad} c_i + \sum_{i=1}^{n-1} h_i \mathbf{J}_i \tag{8}$$

and the enthalpy $h$ is given by

$$h = \sum_i c_i \left[\int_0^T c_{pi}\,\mathrm{d}T + h_i^{(0)}\right]. \tag{9}$$

Equation (7) describes the mass flux of species $i$, due to: (i) the concentration gradient of species $i$ (Flick's Law); (ii) the concentration gradients of all other species (multicomponent diffusion) and (iii) the temperature gradient (thermal diffusion). The coupled heat flux is described by equation (8) where in addition

to the regular Fourier flux, diffusion-thermo (Dufour Effect) and enthalpy transport due to diffusion fluxes are also considered. Here $D_{ij}$ is the diffusion coefficient of species $i$ due to the concentration gradient of species $j$, $D_{iT}$ is the thermal diffusion coefficient of species $i$ due to a temperature gradient, $k$ is the thermal conductivity, $D_{Ti}$ is the diffusion-thermo coefficient due to the concentration gradient of species $i$, $c_{pi}$ is the specific heat of species $i$ and $h^{(0)}$ is the enthalpy of formation.

## 3. A GENERAL 3D ENERGY-SPECIES FIELD TRANSFORMATION

Field transformations for the energy and species equations have been reported by the author for non-reactive [18] and reactive systems [15, 16]. However, these field transformations were limited to steady-state *boundary-layer* equations. In the present study, a general *non-steady three-dimensional* field transformation will be presented. Since there are some similarities between the general 3D transformation, which will be presented below and the *boundary-layer* transformations which were previously reported, many of the details given in refs. [15, 16] and [18] will be avoided here. Thus, in the present paper we will focus only on those mathematical derivations which are unique to 3D equations and are notably different from those in the above mentioned references [15, 16, 18].

With this in mind, we start with the derivation of a 3D kinetic energy equation by multiplying the components of the Navier–Stokes equations (2) (i.e. the components in the $x$, $y$ and $z$ directions, each by its proper velocity component $u$, $v$ and $w$, respectively), and summing up the three resulting scalar equations. This procedure is standard. However, for later use in the present study, it is desired to channel the derivation procedure, so that it will subsequently lead to balance equations of the following mathematical form:

$$\rho \frac{\mathrm{d}}{\mathrm{d}t}(\,) = \operatorname{div}[\mu \operatorname{grad}(\,)] + \dot{s} \tag{10}$$

where $\dot{s}$ is a general source term. To do so, the following mathematical procedures are required.

For example, the momentum equation in the $x$ direction (in Cartesian coordinates) multiplied by $u$, which reads

$$\rho \frac{\mathrm{d}}{\mathrm{d}t}\left(\frac{1}{2}u^2\right) = -u\frac{\partial p}{\partial x} - u\frac{\partial}{\partial x}\left[\left(\frac{2}{3}\mu - \kappa\right)\operatorname{div}\mathbf{V}\right] + u[\operatorname{div}(\mu \operatorname{grad} u)] + u \operatorname{div}\left(\mu \frac{\partial}{\partial x}\mathbf{V}\right) \tag{11}$$

is operated on employing the following mathematical identities:

$$u[\operatorname{div}(\mu \operatorname{grad} u)] = \operatorname{div}\left[\mu \operatorname{grad}\left(\frac{1}{2}u^2\right)\right] - \mu(\operatorname{grad} u)\cdot(\operatorname{grad} u) \tag{12}$$

and

$$\operatorname{div}\left(\mu \frac{\partial}{\partial x}\mathbf{V}\right) = \left(\frac{\partial}{\partial x}\mathbf{V}\right)\cdot(\operatorname{grad}\mu) + \mu\frac{\partial}{\partial x}(\operatorname{div}\mathbf{V}). \tag{13}$$

Thus, via equations (12) and (13), equation (11) may be recast in the following form:

$$\begin{aligned}\rho \frac{\mathrm{d}}{\mathrm{d}t}\left(\frac{1}{2}u^2\right) = {} & -u\frac{\partial p}{\partial x} - u \operatorname{div}\mathbf{V}\frac{\partial}{\partial x}\left(\frac{2}{3}\mu - \kappa\right) \\ & - u\left(\frac{2}{3}\mu - \kappa\right)\frac{\partial}{\partial x}(\operatorname{div}\mathbf{V}) \\ & - \operatorname{div}\left[\mu \operatorname{grad}\left(\frac{1}{2}u^2\right)\right] - \mu(\operatorname{grad} u)\cdot(\operatorname{grad} u) \\ & + u\left(\frac{\partial}{\partial x}\mathbf{V}\right)\cdot(\operatorname{grad}\mu) + \mu u\frac{\partial}{\partial x}(\operatorname{div}\mathbf{V}).\end{aligned} \tag{14}$$

Next, in a similar way, equations are derived to express

$$\frac{\mathrm{d}}{\mathrm{d}t}\left(\frac{1}{2}v^2\right)$$

and

$$\frac{\mathrm{d}}{\mathrm{d}t}\left(\frac{1}{2}w^2\right),$$

via the momentum equations in the $y$ and $z$ directions, respectively. Combining these equations with equation (14) one may identify the 3D dissipation function, see equation (6), which is recast here into the following form

$$\begin{aligned}\Phi = {} & \mu[(\operatorname{grad} u)\cdot(\operatorname{grad} u) + (\operatorname{grad} v) \\ & \cdot(\operatorname{grad} v) + (\operatorname{grad} w)\cdot(\operatorname{grad} w)] \\ & + \left(\frac{1}{3}\mu + \kappa\right)(\operatorname{div}\mathbf{V})^2 + 2\mu G\end{aligned} \tag{15}$$

where $G$ is defined as:

$$G = J\left(\frac{u,v}{y,x}\right) + J\left(\frac{v,w}{z,y}\right) + J\left(\frac{w,u}{x,z}\right). \tag{16}$$

Here, the notation '$J$' is used for a Jacobian.

Then, presenting a function $\Theta$ as

$$\begin{aligned}\Theta = {} & (\tfrac{1}{3}\mu + \kappa)(\operatorname{div}\mathbf{V})^2 + 2\mu G \\ & - (\operatorname{div}\mathbf{V})[\mathbf{V}\cdot\operatorname{grad}(\tfrac{2}{3}\mu - \kappa)] \\ & - (\tfrac{2}{3}\mu - \kappa)\mathbf{V}\cdot[\operatorname{grad}(\operatorname{div}\mathbf{V})] \\ & + [(\mathbf{V}\cdot\operatorname{grad})\mathbf{V}]\cdot\operatorname{grad}\mu + \mu(\mathbf{V}\cdot\operatorname{grad})\operatorname{div}\mathbf{V}\end{aligned} \tag{17}$$

and employing equations (15), (16) and (17), equation (14) is combined with equations of a similar form for

$$\frac{\mathrm{d}}{\mathrm{d}t}\left(\frac{1}{2}v^2\right)$$

and

$$\frac{\mathrm{d}}{\mathrm{d}t}\left(\frac{1}{2}w^2\right)$$

in order to obtain a general 3D kinetic energy equation of the form

$$\rho\frac{\mathrm{d}}{\mathrm{d}t}\left(\frac{1}{2}\mathbf{V}\cdot\mathbf{V}\right)^* = \mathrm{div}\left[\mu\,\mathrm{grad}\left(\frac{1}{2}\mathbf{V}\cdot\mathbf{V}\right)^*\right]+\dot{E}_k^*. \tag{18}$$

The source term in equation (18) is given by

$$\dot{E}_k^* = -\frac{1}{h_\infty}[\mathbf{V}\cdot\mathrm{grad}\,p+\Phi-\Theta] \tag{19}$$

and the kinetic energy is presented in equation (18) in a non-dimensional form defined as

$$\left(\frac{1}{2}\mathbf{V}\cdot\mathbf{V}\right)^* = \frac{1}{h_\infty}\left(\frac{1}{2}\mathbf{V}\cdot\mathbf{V}\right) \tag{20}$$

where $h_\infty$ is the free stream enthalpy.

Next, equation (18) is employed in order to eliminate the dissipation term in the energy equation (4). This leads to the following 'total-energy' balance equation

$$\rho\frac{\mathrm{d}I^*}{\mathrm{d}t} = \mathrm{div}\left[\mathbf{J}_q^*+\mu\,\mathrm{grad}\left(\frac{1}{2}\mathbf{V}\cdot\mathbf{V}\right)^*\right]+\dot{E}_\mathrm{T}^* \tag{21}$$

where the non-dimensional total-energy is defined as

$$I^* = \frac{1}{h_\infty}\left[h+\frac{1}{2}(\mathbf{V}\cdot\mathbf{V})\right] \tag{22}$$

and where

$$\dot{E}_\mathrm{T}^* = \frac{1}{h_\infty}\left(\frac{\partial p}{\partial t}+\Theta\right). \tag{23}$$

The energy equation (21) and the species equations (3) are both coupled to the velocity field $\mathbf{V}$ and intercoupled through the transport fluxes as expressed by equations (7) and (8). Thus, it is desirable to transform the energy and species equations into a set of equations which describes a combined 'energy-species' field in a mathematical form that makes it suitable for solution by standard numerical codes. Such a field transformation is carried out as follows:

First, we present a column state vector with $(n+1)$ components defined as:

$$\xi = \begin{bmatrix} c_1 \\ c_2 \\ \vdots \\ c_{n-1} \\ I^* \\ \frac{1}{2}(\mathbf{V}\cdot\mathbf{V})^* \end{bmatrix}. \tag{24}$$

Then, the kinetic energy equation (18), the total energy equation (21), and the species equations (3) are re-expressed in terms of $\xi$. That is, the kinetic energy equation takes the following form

$$\rho\frac{\mathrm{d}}{\mathrm{d}t}\left(\frac{1}{2}\mathbf{V}\cdot\mathbf{V}\right)^* = \mathrm{div}\,[\mu\,\omega_k\,\mathrm{grad}\,\xi]+\dot{E}_k^* \tag{25}$$

where $\omega_k$ is a row vector give by

$$\omega_k = [0,0,0,\ldots,0,1]. \tag{26}$$

To treat the energy equation in a similar way, it is imperative first to re-express the total energy flux, as described by equations (7), (8) and (21), in terms of $\xi$. To do so, we employ here the definitions of equivalent transport coefficients and non-dimensional groups as given in ref. [18]. These are the 'equivalent energy conductivity' $\bar{k}$, the 'equivalent diffusion-thermo coefficient' $\bar{D}_j$, and the equivalent Prandtl and Lewis numbers which are defined as:

$$\bar{k} = k+\sum_{j=1}^{n-1} h_j D_{jT} \tag{27}$$

$$\bar{D}_j = \frac{1}{\rho h_j}\left(D_{\mathrm{T}j}+\sum_{i=1}^{n-1} h_i D_{ij}\right) \tag{28}$$

$$\bar{P}r = \frac{c_{\mathrm{pf}}\mu}{\bar{k}} \tag{29}$$

$$\bar{L}e_j = \frac{\rho\bar{D}_j c_{\mathrm{pf}}}{\bar{k}}. \tag{30}$$

Thus, by substituting equation (7) into equation (8) and making use of the above definitions, equation (21) finally becomes

$$\rho\frac{\mathrm{d}I^*}{\mathrm{d}t} = \mathrm{div}\,[\mu\omega_\mathrm{T}\,\mathrm{grad}\,\xi]+\dot{E}_\mathrm{T}^* \tag{31}$$

where

$$\omega_\mathrm{T} = \left[\frac{1}{\bar{P}r}(\bar{L}e_1-1)\frac{h_1}{h_\infty};\quad \ldots\frac{1}{\bar{P}r}(\bar{L}e_{n-1}-1)\frac{h_{n-1}}{h_\infty};\right.$$
$$\left.\frac{1}{\bar{P}r}(\bar{P}r-1)\right]. \tag{32}$$

Next, the species equations (3) are operated on in a similar way. Again, we employ definitions of equivalent transport coefficients and non-dimensional groups, specifically those which are related to the coupled diffusion flux, i.e. the 'equivalent diffusion'

and the 'equivalent thermal-diffusion' coefficients which are defined respectively as [18]:

$$\bar{D}_{ij} = D_{ij} - \frac{D_{i\mathrm{T}}}{c_{\mathrm{pf}}} h_j \tag{33}$$

$$\bar{D}_{i\mathrm{H}} = \frac{D_{i\mathrm{T}}}{c_{\mathrm{pf}}} h_\infty. \tag{34}$$

These equivalent coefficients lead to the definitions of an equivalent diffusional Schmidt number and an equivalent thermal diffusion Schmidt number, which are respectively given by:

$$\bar{S}c_{ij} = \frac{\mu}{\bar{D}_{ij}} \tag{35}$$

$$\bar{S}c_{i\mathrm{H}} = \frac{\mu}{\bar{D}_{i\mathrm{H}}}. \tag{36}$$

Then, subject to the above definitions, equation (3) may be recast into the following form

$$\rho \frac{\mathrm{d}c_i}{\mathrm{d}t} = \mathrm{div}\,[\mu \omega_{c_i} \,\mathrm{grad}\,\xi] + \dot{v}_i \tag{37}$$

$$\omega_{c_i} = \left[\frac{1}{\bar{S}c_{i,1}};\ \frac{1}{\bar{S}c_{i,2}};\ \ldots \frac{1}{\bar{S}c_{i,n-1}};\ \frac{1}{\bar{S}c_{i\mathrm{H}}};\ -\frac{1}{\bar{S}c_{i\mathrm{H}}}\right]. \tag{38}$$

Now, it is convenient to combine the conservation equations (25), (31) and (37) to form the following single matrix equation

$$\rho \frac{\mathrm{d}}{\mathrm{d}t} \xi = \mathrm{div}(\mu \mathbf{\Omega} \,\mathrm{grad}\,\xi) + \dot{\mathbf{S}} \tag{39}$$

where $\mathbf{\Omega}$ is the nonsymmetrical $(n+1 \times n+1)$ square matrix formed by the row matrices $\omega_{c_i}$, $\omega_{\mathrm{T}}$ and $\omega_k$ [see equations (26), (32) and (38)], and $\dot{\mathbf{S}}$ is a column vector formed by the scalar source terms $\dot{v}_i$ $(i = 1, 2, \ldots n-1)$, $\dot{E}^*_{\mathrm{T}}$ and $\dot{E}^*_k$:

$$\dot{\mathbf{S}} = [v_1, v_2, \ldots v_{n-1}, \dot{E}^*_{\mathrm{T}}, \dot{E}^*_k]^{\mathrm{T}}. \tag{40}$$

Next, standard mathematical procedures such as described in ref. [18] and summarized here in the Appendix, enable us to employ equation (39) and derive a combined 'energy-species' field with $n$ elements of the form

$$\zeta_i = \sum_{j=1}^{n-1} \alpha_{ij} c_j + \beta_i \left(h + \frac{1}{2}\mathbf{V}\cdot\mathbf{V}\right)^* \quad i = 1, 2, \ldots n \tag{41}$$

which is governed by the following general 3D balance equation

$$\rho \frac{\mathrm{d}}{\mathrm{d}t}\zeta_i = \mathrm{div}\left[\frac{\mu}{\tilde{P}r_i}\,\mathrm{grad}\,\zeta_i + \frac{\mu}{\tilde{P}r_i}(\tilde{P}r_i - 1)\,\mathrm{grad}\,\frac{1}{2}(\mathbf{V}\cdot\mathbf{V})^*\right] + \sum_{j=1}^{n-1} \alpha_{ij}\dot{v}_j + \beta_i \dot{E}^*_{\mathrm{T}} \quad (i-1, 2, \ldots n). \tag{42}$$

The coefficients $\alpha_{ij}$ and $\beta_i$ are defined in terms of the elements of the inverse modal matrix of $\mathbf{\Omega}$ (see Appendices A and B), and $\tilde{P}r_i$ denotes the equivalent Prandtl–Schmidt numbers which are defined in terms of the eigenvalues of $\mathbf{\Omega}$.

The set of $n$ equations presented by equation (42) replaces: the original $(n-1)$ species conservation equations (3) and the original energy equation (4), which are inter-coupled through their diffusion and energy transport fluxes. The advantage of using the set derived above, equation (42), instead of the original equations (3) and (4) for analysing coupled effects is that it allows one to obtain solutions for $\zeta_i$ via classical solution procedures (as demonstrated in the next section) and to return to the physical fields $c_i$ and $h$ via

$$c_i = \sum_{j=1}^{n} \gamma_{ij}\zeta_j \tag{43}$$

$$h^* = \sum_{j=1}^{n} \gamma_j \zeta_j - \frac{1}{2}(\mathbf{V}\cdot\mathbf{V})^* \tag{44}$$

where the coefficients $\gamma_{ij}$ and $\gamma_i$ are also defined in the Appendix.

## 4. TRANSIENT TRANSPORT IN 3D (AND 2D) STAGNATION FLOWS

In this section, we will analyse the transient coupled diffusion and energy transport to surfaces which are subject to a sudden change (step function) in temperature and species concentrations. Attention is directed in the present study to the unsteady transport fluxes in a 3D (and 2D) stagnation flow where the flow itself is steady. Thus, we will focus on the boundary conditions and solution procedure for the transformed 'energy-species' equation (42). We denote by O the stagnation point of a general 3D surface. At O, we attach a curved orthogonal coordinate system with axis: $e_1$, $e_2$ and $e_3$, where the coordinate normal to the surface $\bar{n}(\equiv e_1)$ is opposite to the direction of the free stream flow velocity. Next, we use the following simplifying assumptions:

(a) the dominant flux of $\zeta_i$, is in the normal $(\bar{n})$ direction, whereas the energy and diffusion fluxes in the $e_2$ and $e_3$ directions are negligible.

(b) Gas-phase chemical reactions are not considered here, i.e. $v_j = 0$.

(c) $\partial p/\partial t = 0$, that is the pressure is steady. It should be noted that this assumption still allows non-zero pressure gradients in all directions.

(d) Bulk viscosity effects and the function $\Theta$ are neglected.

Subject to the above assumptions, the transformed 'energy-species' equation (42) becomes:

$$\rho \frac{\partial \zeta_i}{\partial t} + \rho \mathbf{V} \cdot \left[\frac{1}{h_1}\frac{\partial \zeta_i}{\partial \bar{n}}\hat{n} + \frac{1}{h_2}\frac{\partial \zeta_i}{\partial e_2}\hat{e}_2 + \frac{1}{h_3}\frac{\partial \zeta_i}{\partial e_3}\hat{e}_3\right]$$

$$= \frac{1}{h_1 h_2 h_3}\left[\frac{\partial}{\partial \bar{n}}\left(\frac{h_2 h_3}{h_1}\frac{\mu}{\tilde{P}r_i}\frac{\partial \zeta_i}{\partial \bar{n}}\right)\right]$$

$$+\operatorname{div}\left[\frac{\mu}{\tilde{P}r_i}(\tilde{P}r_i - 1)\operatorname{grad}\frac{1}{2}(\mathbf{V}\cdot\mathbf{V})^*\right] \quad (45)$$

where $\hat{e}_1$, $\hat{e}_2$ and $\hat{e}_3$ are unit vectors in the $e_1$, $e_2$ and $e_3$ directions, respectively. The coefficients $h_1$, $h_2$ and $h_3$ are scale coefficients, where, for example, for a cylindrical surface of radius $R$, in a cross flow (for cylindrical coordinates $\bar{n}$, $\phi$ and $z$)

$$h_1 = h_{\bar{n}}(\equiv h_r) = 1; \quad h_2 = h_\phi = (\bar{n}+R); \quad h_3 = h_z = 1;$$

and for a spherical surface of radius $R$ (in spherical coordinates $\bar{n}$, $\theta$ and $\phi$):

$$h_1 = h_{\bar{n}}(\equiv h_r) = 1; \quad h_2 = h_\theta = (\bar{n}+R);$$

$$h_3 = h_\phi = (\sin\theta).$$

The boundary and initial conditions for the 'energy-species' equations are as follows:

$$\text{at } \bar{n} \to \infty: \quad c_i(\infty, e_2, e_3, t) = c_{i,\infty},$$

$$T_0(\infty, e_2, e_3, t) = T_{0,\infty} \quad (46)$$

and for a step change in enthalpy and species concentrations at the surface we have

$$h_0(0, e_2, e_3, t) = h_{0,\infty} + (h_{0,w} - h_{0,\infty})\mathscr{H}(t) \quad (47)$$

and

$$c_i(0, e_2, e_3, t) = c_{i,\infty} + (c_{i,w} - c_{i,\infty})\mathscr{H}(t) \quad (48)$$

where $\mathscr{H}(t)$ is the Heaviside unit operator which equals zero for $t < 0$ and unity for $t \geqslant 0$.

Solutions for the transient fluxes are presented in terms of the following non-dimensional field variable

$$\phi_i = \frac{\zeta_i - \zeta_{i\infty}}{\zeta_{iw} - \zeta_{i\infty}} = \frac{\zeta_i - \sum_{j=1}^{n-1}\alpha_{ij}c_{j\infty} - \beta_i h^*_\infty}{\sum_{j=1}^{n-1}\alpha_{ij}(c_{jw} - c_{j\infty}) + \beta_i(h^*_w - h^*_\infty)}. \quad (49)$$

For each $\zeta_i$ we define a non-dimensional time variable as

$$\tau_i = \tau\frac{Pr}{\tilde{P}r_i}. \quad (50)$$

Here $\tau$ is the *general* non-dimensional time variable:

$$\tau = \frac{2^\varepsilon Kt}{Pr} \quad (51)$$

where for a two-dimensional problem $\varepsilon = 0$, and $K = 2U_\infty/R$ for a cylindrical surface of radius $R$; for a 3D problem $\varepsilon = 1$, and $K = 3U_\infty/2R$ for a spherical shape surface of radius $R$.

Thus, according to equations (44), (49) and (50) the transient coupled surface heat flux is given by

$$J_{qw} = h_\infty \sum_{i=1}^{n}\frac{\mu}{\tilde{P}r_i}\gamma_i(\zeta_{iw} - \zeta_{i\infty})\phi'(0,\tau_i)$$

$$= h_\infty \sum_{i=1}^{n}\frac{\mu}{\tilde{P}r_i}\gamma_i\left[\sum_{j=1}^{n-1}\alpha_{ij}(c_{jw} - c_{j\infty}) + \beta_i(h^*_w - h^*_\infty)\right]\phi'(0,\tau_i) \quad (52)$$

where the prime denotes differentiation with respect to $\bar{n}$.

Finally, to enable presentation of general multicomponent solutions, we present here a general transport coupling parameter $F$. This parameter represents the contribution of transport-coupling effects to the surface heat flux for a multicomponent mixture, normalized by the contribution of these effects to the surface heat flux for a binary mixture for which solutions are widely reported in the literature (e.g. a mixture of hydrogen and nitrogen, or helium nitrogen, see refs. [1–7]). That is

$$F = \frac{\sum_{i=1}^{n}\gamma_i\left[\frac{Pr}{\tilde{P}r_i}\right]\frac{\phi'(0,f_w,\tilde{P}r_i)}{\phi'(0,f_w,Pr)}\left[\sum_{j=1}^{n}\alpha_{ij}\frac{c_{je} - c_{jw}}{h^*_e - h^*_w}\right]}{\left[\gamma_1\left(\frac{Pr}{\tilde{P}r_1}\right)\frac{\phi'(0,f_w,\tilde{P}r_1)}{\phi'(0,f_w,Pr)}\alpha_{11} + \gamma_2\left(\frac{Pr}{\tilde{P}r_2}\right)\frac{\phi'(0,f_w,\tilde{P}r_2)}{\phi'(0,f_w,Pr)}\alpha_{21}\right]\frac{c_{1e} - c_{1w}}{h^*_e - h^*_w}} \quad (53)$$

where $f_w$ is the wall injection parameter defined as

$$f_w = \frac{-(\rho v)_w}{(\rho\mu)^{1/2}_\infty\left[\frac{1}{2}\left(\frac{1}{h_2}\frac{\partial U_\infty}{\partial e_2} + \frac{1}{h_3}\frac{\partial U_\infty}{\partial e_3}\right)\right]^{1/2}_w}\left(\frac{1}{\varepsilon+1}\right)^{1/2}. \quad (54)$$

The procedure by which the equivalent Prandtl–Schmidt numbers $\tilde{P}r_i$, and the coefficients $\alpha_{ij}$, $\beta_i$ and $\gamma_i$ are evaluated is described in Appendix A, where examples of computed numerical values for these coefficients for various gas mixtures are listed in Appendix B. The transport coefficients are calculated according to the molecular theory of gases: the diffusion coefficients are evaluated on the basis of the Lennard–Jones model [27] and for the thermal diffusion ratio, the modified hard-sphere model is used [28]. All transport properties are treated as variables and are evaluated according to the local temperature and species concentrations. Calculated results are presented and discussed in the next section.

## 5. RESULTS AND DISCUSSION

Calculations are carried out for a flow of nitrogen at a free stream Mach number $M_\infty = 3.5$. For nitrogen–hydrogen mixtures, various mass flow rates of hydrogen are injected at the wall. For multicomponent mix-

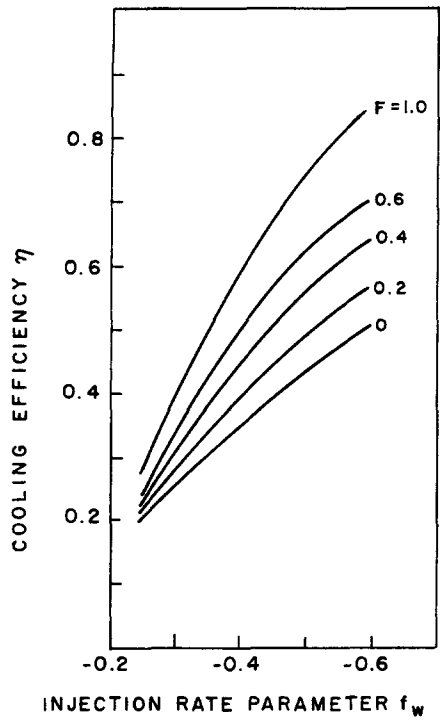


Fig. 1. Effects of the multicomponent transport-coupling parameter $F$ and surface injection rates on final steady-state cooling efficiency $\eta$.

tures of nitrogen and other chemical species such as $H_2$, He, CO, Ar, the mass of the injected hydrogen is replaced by the combined masses of these other species. Additional data is given in Appendix B. We begin here with the results for the 3D steady-state wall injection cooling efficiency, followed by a discussion of the transient multicomponent effects which subsequently lead to these steady-state conditions. The cooling efficiency is denoted here by $\eta$

$$\eta = \frac{J_{qw}^{NC} - J_{qw}^{C}}{J_{qw}^{NC}} (\tau \to \infty) \tag{55}$$

which is the ratio of the transport-coupling contribution to the wall heat flux, and the wall heat flux for a non-coupled (N.C.) case without surface injection, after reaching steady-state conditions.

General multicomponent results are presented in Fig. 1 for the final steady-state values of $\eta$, the cooling efficiency, which is affected by a wide range of wall injection rates, $f_w$, of various gas mixtures (see examples in Appendix B) which are represented by various values of the parameter $F$. This transport coupling parameters, see equation (53) and properties given in the appendix, represents a wide range of transport properties of multicomponent mixtures. The value $F = 0$ represents, by definition, no thermodynamic coupling effects since it refers to a situation in which the injected cooling gas is of the same chemical composition as the free-stream gas (i.e. injection of nitrogen into a nitrogen stream). At the other end: $F = 1$ represents, by definition, injection of the lightest molecule, i.e. injection of pure hydrogen into a pure nitrogen stream.

Examples of computed numerical values for the equivalent Prandtl numbers $\tilde{Pr}_i$ and the coefficients $\alpha_{ij}$ and $\gamma_i$, for various gas mixtures are presented in Appendix B. These coefficients are needed for the evaluation of the parameter $F$, see equation (53). First we examine some trivial cases. For example, injection of the gas CO into a nitrogen stream is expected to be characterized by an $F$ value which approaches zero, since the properties of CO are very similar to the properties of $N_2$ (see ref. [21]). Indeed, for the $N_2$–CO mixture (listed in Appendix B as case No. 1), we have computed here and obtained $F = (1.1346 \times 10^{-2}/3.2817) = 0.0035$, where the denominator in the expression for $F$ [see equation (53)] was evaluated for an $N_2$–$H_2$ mixture (listed as case No. 2 in Appendix B).

Another case at the other end of the spectrum for $F$ is examined as follows. If instead of a binary mixture of: 0.2 $N_2$ + 0.8 $H_2$ (given in mass fractions), we evaluate a trinary mixture of: 0.2 $N_2$ + 0.65 $H_2$ + 0.15 He (case No. 3 in Appendix B), we would expect an $F$ value which is close to unity, since a fraction of the hydrogen is replaced by a heavier gas, helium. Again via equation (53), we obtain or the above case: $F = (2.6095/3.2817) = 0.795$. Increasing the hydrogen concentrations at the expense of the helium in the mixture shifts the $F$ value towards unity. On the other hand, replacing the hydrogen in the mixture completely by helium (see case No. 4 in Appendix B) results in a drastic decrease of the $F$ value from 0.795 to 0.427.

Next, on the basis of the above analysis, we discuss the results plotted in Fig. 1. As shown in Fig. 1, one can obtain a desired final steady-state cooling efficiency through various injection rates, depending on the properties of the injected gas. For example, a desired steady-state cooling efficiency of $\eta = 0.4$ can be obtained by injection of nitrogen into nitrogen at a rate of $f_w = -0.458$, or hydrogen into nitrogen at a much lower rate of $f_w = -0.301$ (see Fig. 1). In the case of multicomponent mixtures, and that is one of the new contributions of the present study, the desired steady-state cooling efficiency can be also obtained through specifying the *combined values* of the injection rate and the transport properties of multicomponent mixtures as expressed by the parameter $F$. For example, $\eta = 0.4$ can be obtained for multicomponent mixtures through the following operating conditions: (i) for a mixture of: 0.2 $N_2$ + 0.65 $H_2$ + 0.15 He, via an injection rate of $f_w = -0.318$, or (ii) for a mixture of: 0.2 $N_2$ + 0.45 He + 0.25 $H_2$ + 0.1 CO, via a higher injection rate $f_w = -0.357$, etc. For the above cases, (i) and (ii), the parameter $F$ equals 0.795 and 0.451, respectively. Hence, according to Fig. 1, the aforementioned injection rates both correspond to a cooling efficiency of $\eta = 0.4$.

The transient multicomponent effects are discussed

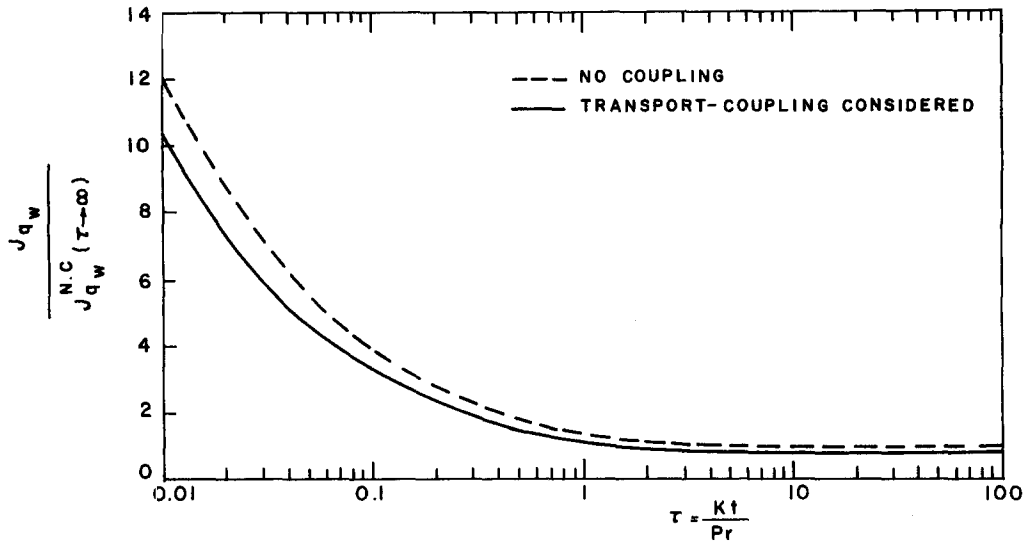


Fig. 2. Evolution of the transport surface heat flux: (i) —— transport-coupling considered, (ii) --- transport-coupling neglected. (Both fluxes are normalized by the non-coupled steady-state heat flux.)

next. In Fig. 2, a coupled transient case which leads to a final steady-state cooling efficiency $\eta = 0.19$ is presented. The evolution of the coupled transient surface heat flux is compared with a non-coupled (i.e. mono-component without surface injection) case. Both fluxes are normalized by the non-coupled steady-state heat flux and are plotted as a function of the non-dimensional time variable $\tau$. Generally, the transient coupled-surface-heat-flux exhibits a pattern similar to the non-coupled one, that is, it decreases monotonically with time until it reaches a steady-state value. The *absolute* cooling due to the transport coupling effects

$$\frac{J^{NC}_{qw}(\tau) - J^{C}_{qw}(\tau)}{J^{NC}_{qw}(\tau \to \infty)} \tag{56}$$

i.e. the reduction of surface heat flux in *absolute* values (normalized by non-coupled steady-state heat flux) is significantly larger at short latencies [as indicated also in Fig. 3(a)]. This is attributed to the fact that the largest contribution of the transport-coupling effects to the surface heat flux in *absolute values*, obviously occurs when the concentration gradients are most pronounced.

The above, however, does not contradict the results shown in Fig. 3(b), where the contribution of the transport-coupling effects *relative to the instantaneous* surface heat flux exhibits *local overshoots* instead of a monotonic increase. The trend in Fig. 3(b) may be explained as follows: the relative contribution of the transport-coupling effects depends not only on the magnitude of the Soret (thermal-diffusion) and Dufour (diffusion-thermo) cross-coupling coefficients, which are usually much smaller than the regular (Fourier's and Fick's) transport coefficients, but also on the *relative* magnitude of the local species concentration gradients with respect to the local temperature gradient, multiplied by the proper transport coefficients, see equations (7), (8), (27) and (28). These are expressed by a multicomponent 'Transport-coupling Activity' (TA) number:

$$\mathrm{TA} = \frac{\sum_{j=1}^{n-1} \frac{1}{\rho h_j}\left(D_{Tj} + \sum_{j=1}^{n-1} h_i D_{ij}\right)\frac{\partial c_j}{\partial \bar{n}}}{\left(k + \sum_{j=1}^{n-1} h_j D_{jT}\right)\frac{\partial T}{\partial \bar{n}}} = \frac{J^{NC}_{qw}(\tau) - J^{C}_{qw}(\tau)}{J^{NC}_{qw}(\tau)}. \tag{57}$$

Note that at $\tau \to \infty$ the value of the non-dimensional transport-coupling activity number approaches the steady-state cooling efficiency $\eta$ [see equation (55) and also in Fig. 3(b)]. Although the magnitudes of all gradients (species-concentrations and temperature) generally decrease with time, they decrease at different characteristic rates and may also evidence local overshoot values as indicated in previous studies [14, 20]. For example, Inger [14] analysed the effects of thermal-diffusion on oxygen concentration distributions near intense fires and using a simple theoretical model, he showed that these effects may cause local 'overshoots' relative to ambient conditions. Another example of local temperature overshoots due to transport coupling of heat and moisture in composite materials, which are in agreement with experimental data, was presented by Tambour [20]. Although the characteristic transport coefficients are different from those used for gases, the basic phenomena are essentially of the same nature, as discussed in ref. [20].

Thus, although the transport coupling effects are significantly larger at short latencies, relative to the local Fourier heat flux which is also much larger at short latencies, the cooling efficiency (i.e. the ratio between the two) is smaller than that finally obtained

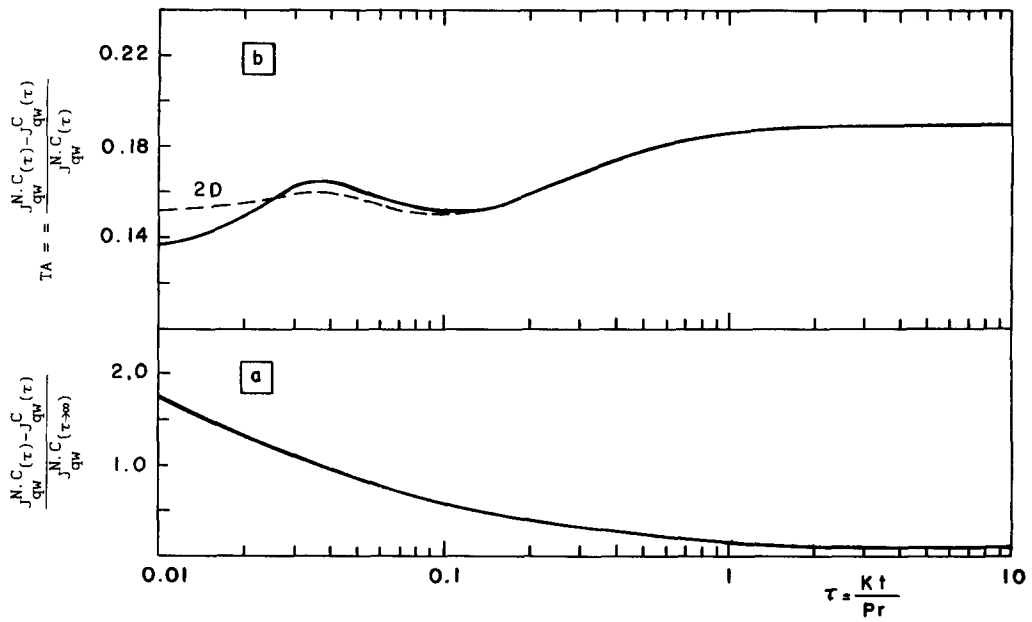


Fig. 3. Transient behavior of the transport coupling contribution to the surface heat flux: (a) normalized by the *steady-state* non-coupled surface heat flux. (b) Normalized by the *transient* non-coupled surface heat flux, i.e. equal to the 'Transport-coupling Activity' number: 'TA', see equation (57). [A two-dimensional case which leads to the same final steady-state cooling efficiency is presented by a dotted line in (b).]

when the system reaches steady-state conditions [see Fig. 3(b)]. However, the cooling efficiency does not increase monotonically with time, but is subject to local fluctuations expressed by fluctuating values of the Transport-coupling Activity number, which is due to local overshoots in temperatures and species concentrations as expressed by equation (57). Similar local over-shoots were obtained in the present study for a 2D case of the same final steady-state cooling efficiency [see Fig. 3(b)].

Future research will examine the effects of these *transient* transport-coupling phenomena on spray vaporization and spray flames. Studies in this field have recently been carried out (e.g. see refs. [22, 25, 26]) without taking into account transport-coupling effects.

## REFERENCES

1. J. R. Baron, Thermodynamic coupling in boundary-layers, *Am. Rocket Soc. J.* **32**, 1053–1059 (1962).
2. J. R. Baron, Thermal diffusion effects in mass transfer, *Int. J. Heat Mass Transfer* **6**, 1025–1034 (1963).
3. E. R. G. Eckert, W. J. Minkowycz, E. M. Sparrow and W. E. Ibele, Heat transfer and friction in two-dimensional stagnation flow of air with helium injection, *Int. J. Heat Mass Transfer* **6**, 245–249 (1963).
4. E. M. Sparrow, W. J. Minkowycz and E. R. G. Eckert, Diffusion-thermo effects in stagnation-point flow of air with injection of gases of various molecular weights into the boundary layer, *AIAA J.* **2**, 652–659 (1964).
5. E. M. Sparrow, W. J. Minkowycz, E. R. G. Eckert and W. E. Ibele, The effect of diffusion-thermo and thermal diffusion for helium injection into plane and axisymmetric stagnation flow of air, *J. Heat Transfer, Trans. ASME Ser. C* **86**, 311–319 (1964).
6. W. N. Gill, E. del Casal and S. W. Zeh, Binary diffusion and heat transfer in laminar free convection boundary layers on a vertical plate, *Int. J. Heat Mass Transfer* **8**, 1135–1151 (1965).
7. A. Atimtay and W. N. Gill, The effect of free stream concentration on heat and binary mass transfer with thermodynamic coupling in forced convection on a flat plate, *Chem. Engng Sci.* **36**, 1001–1008 (1981).
8. R. Taylor, Coupled heat and mass transfer in multicomponent systems: solution of the Maxwell–Stefan equations, *Lett. Heat Mass Transfer* **8**, 405–416 (1981).
9. R. Srivastava and D. E. Rosner, A new approach to the correlation of boundary layer mass transfer rates with thermal diffusion and/or variable properties, *Int. J. Heat Mass Transfer* **22**, 1281–1294 (1979).
10. D. E. Rosner, Thermal (Soret) diffusion effects on interfacial mass transport rates, *PhysicoChem. Hydrodyn.* **1**, 159–185 (1980).
11. D. E. Rosner, Convective diffusion as an intruder in kinetic studies of surface catalyzed reactions, *AIAA J.* **2**, 593–610 (1964).
12. D. E. Rosner, *Transport Processes in Chemically Reacting Flow Systems*. Butterworths, London (1986).
13. P. M. Chung, Chemically frozen boundary-layer with surface reactions behind a strong moving shock, *Physics Fluids* **6**, 550–559 (1963).
14. G. R. Inger, Simple model of convection–diffusion coupling near flames, *Physics Fluids* **19**, 1642–1644 (1976).
15. Y. Tambour, Transport coupling theory for multicomponent non-equilibrium chemically reacting boundary layers, *Physics Fluids* **22**, 1255–1260 (1979).
16. Y. Tambour and B. Gal-Or, Theory of thermodynamic coupling in surface reacting boundary layers, *Physics Fluids* **20**, 880–887 (1977).
17. Y. Tambour, On thermal-diffusion effects in chemically frozen multicomponent boundary layer with surface catalytic recombination behind a strong moving shock, *Int. J. Heat Mass Transfer* **23**, 321–327 (1980).
18. Y. Tambour and B. Gal-Or, Phenomenological theory of thermodynamic coupling in multicomponent, compressible laminar boundary layers, *Physics Fluids* **19**, 219–226 (1976).

19. Y. Tambour, F. Anidjar and J. B. Greenberg, Bulk viscosity effects in radially expanding flows, in preparation.
20. Y. Tambour, On local temperature overshoots due to transport coupling of heat and moisture in composite materials, *J. Comp. Mater.* **18,** 478–494 (1984).
21. Y. Tambour and L. G. Cherulnec, Thermodynamically coupled heat transfer to ablative graphite surfaces in supersonic $CO_2$–$N_2$ gas streams, *Chem. Engng Commun.* **43,** 119–132 (1986).
22. Y. Tambour, Transient mass and heat transfer from a cloud of vaporizing droplets of various size distributions: a sectional approach, *Chem. Engng Commun.* **44,** 183–196 (1986).
23. Y. Tambour, A Lagrangian sectional approach for simulating droplet size distribution of vaporizing fuel sprays in a turbulent jet, *Combust. Flame* **60,** 15–28 (1985).
24. Y. Tambour, Vaporization of polydisperse fuel sprays in a laminar boundary layer flow: a sectional approach, *Combust. Flame* **58,** 103–114 (1984).
25. I. Silverman, J. B. Greenberg and Y. Tambour, Asymptotic analysis of a premixed polydisperse spray flame, *SIAM J. Appl. Math.* **51,** 1284–1303 (1991).
26. D. Katoshevski and Y. Tambour, Theoretical study of multisize evaporating sprays in a free shear-layer flow, *Phys. Fluids A* **5,** 3085–3098 (1993).
27. J. O. Hirschfelder, C. F. Curtiss and R. B. Bird, *Molecular Theory of Gases and Liquids.* John Wiley, New York (1954).
28. J. O. Chapman and T. G. Cowling, *The Mathematical Theory of Non-Uniform Gases.* Cambridge University Press, Cambridge (1952).

## APPENDIX A

A summary of the derivation procedure, the definitions and numerical data of the direct and cross-coupling transport coefficients: $\tilde{Pr}_i$, $\alpha_{ij}$, $\beta_i$, $\gamma_{ij}$, $\gamma_i$ for the multicomponent combined 'enegy-species' field $\zeta_i$ are given below.

First, the equivalent Prandtl–Schmidt numbers $\tilde{Pr}_i$ are defined as

$$\tilde{Pr}_i = \frac{1}{\lambda_i} \tag{A1}$$

where $\lambda_i$ are the eigenvalues of the non-symmetrical coefficient matrix $\boldsymbol{\Omega}$, which is formed by the row matrices $\boldsymbol{\omega}_c$, $\boldsymbol{\omega}_T$ and $\boldsymbol{\omega}_k$; see equations (38), (32) and (26).

Then we denote by $\boldsymbol{\Lambda}$ a diagonal matrix with elements $\lambda_i$

$$\boldsymbol{\Lambda} = \mathrm{diag}(\lambda_1, \lambda_2, \ldots \lambda_{n+1}); \tag{A2}$$

and since the eigenvalues $\lambda_i$ are distinct [18]

$$\boldsymbol{\Lambda} = \mathbf{M}^{-1}\boldsymbol{\Omega}\mathbf{M}. \tag{A3}$$

Here $\mathbf{M}$ and $\mathbf{M}^{-1}$ are the modal and the inverse-modal matrices of $\boldsymbol{\Omega}$, respectively.

Next, denoting the elements of the inverse-modal matrix by $\mu_{ij}$, that is

$$\mathbf{M}^{-1} = [\mu_{ij}] \tag{A4}$$

enables one to express the coefficients $\alpha_{aj}$ and $\beta_i$ in terms of $\mu_{ij}$, as follows

$$\alpha_{ij} = \frac{\mu_{ij}}{-\mu_{i,n+1}} \quad \text{and} \quad \beta_i = \frac{\mu_{i,n}}{-\mu_{i,n+1}}. \tag{A5}$$

Finally, constructing the following coefficient determinant

$$\Delta = |\alpha_{ij}, \beta_i| = \begin{bmatrix} \alpha_{1,1} & \alpha_{1,2} & \cdots & \alpha_{1,n-1,} & \beta_1 \\ \alpha_{2,1} & \alpha_{2,2} & \cdots & \alpha_{2,n-1,} & \beta_2 \\ \vdots & \vdots & & \vdots & \vdots \\ \alpha_{n,1} & \alpha_{n,2} & \cdots & \alpha_{n,n-1} & \beta_n \end{bmatrix} \tag{A6}$$

and denoting the cofactors; of the $j$th column by $C^{(i,j)}$, enables one to express the coefficients $\gamma_{ij}$ and $\gamma_i$ in terms of $C^{(i,j)}$:

$$\gamma_{ij} = \frac{C^{(i,j)}}{\Delta} \quad \text{and} \quad \gamma_i = \frac{C^{(i,n)}}{\Delta}. \tag{A7}$$

## APPENDIX B

Examples of computed numerical values for the equivalent Prandtl–Schmidt numbers $\tilde{Pr}_i$ and the coefficients $\alpha_{ij}$ and $\gamma_i$, for various gas mixtures are given below.

*Mixture No.* 1: 0.2 $N_2$+0.8 CO (given in mass fractions)
Temperature 1034 K
Prandtl number of the mixture: 0.75232
Schmidt number = 0.74601

matrix $\boldsymbol{\Omega}$ =

$$\begin{bmatrix} 1.322\times10^{0} & 4.788\times10^{-3} & -4.788\times10^{-3} \\ -1.885\times10^{-2} & 1.348\times10^{0} & -3.481\times10^{-1} \\ 0 & 0 & 1 \end{bmatrix}$$

$\tilde{Pr}_1 = 0.75436$ $\quad \alpha_{1,1} = -4.696\times10^{0}$

$\tilde{Pr}_2 = 0.74399$ $\quad \alpha_{2,1} = -8.383\times10^{-1}$

$\tilde{Pr}_3 = 1$ $\quad \beta_i = 1$

$\gamma_1 = -2.173\times10^{-1}$ $\quad \gamma_{1,1} = -2.592\times10^{-1}$

$\gamma_2 = 1.217\times10^{0}$ $\quad \gamma_{1,2} = 2.592\times10^{-1}$.

*Mixture No.* 2: 0.2 $N_2$+0.8 $H_2$ (given in mass fractions)
Temperature 1034 K
Prandtl number of the mixture = 0.67706
Schmidt number: 1.2314

matrix $\boldsymbol{\Omega}$ = $\begin{bmatrix} 8.97\times10^{-1} & 8.55\times10^{-3} & -8.55\times10^{-3} \\ 6.06\times10^{0} & 1.40\times10^{0} & -3.95\times10^{-1} \\ 0 & 0 & 1 \end{bmatrix}$

$\tilde{Pr}_1 = 6.743\times10^{-1}$ $\quad \alpha_{1,1} = 1.035\times10^{1}$

$\tilde{Pr}_2 = 1.236\times10^{0}$ $\quad \alpha_{2,1} = -6.850\times10^{1}$

$\tilde{Pr}_3 = 1$ $\quad \beta_i = 1$

$\gamma_1 = 8.688\times10^{-1}$ $\quad \gamma_{1,1} = 1.268\times10^{-2}$

$\gamma_2 = 1.312\times10^{-1}$ $\quad \gamma_{1,2} = -1.268\times10^{-2}$.

*Mixture No.* 3: 0.2 $N_2$+0.65 $H_2$+0.15 He (given in mass fractions)
Temperature 1034 K
Prandtl number of the mixture: 0.67234
Schmidt numbers: 1.3779; 1.2427; 0.61322

$\boldsymbol{\Omega}$ =

$$\begin{bmatrix} 8.70\times10^{-1} & -5.65\times10^{-3} & 8.73\times10^{-3} & -8.73\times10^{-3} \\ 1.71\times10^{-1} & 1.62\times10^{0} & 1.69\times10^{-3} & -1.69\times10^{-3} \\ 5.38\times10^{0} & -7.16\times10^{-2} & 1.40\times10^{0} & -3.93\times10^{-1} \\ 0 & 0 & 0 & 1 \end{bmatrix}$$

$\tilde{P}r_1 = 6.20 \times 10^{-1}$ $\alpha_{1,1} = 1.7 \times 10^{1}$

$\tilde{P}r_2 = 6.78 \times 10^{-1}$ $\alpha_{1,2} = 9.15 \times 10^{0}$

$\tilde{P}r_3 = 1.26 \times 10^{0}$ $\alpha_{1,3} = -6.87 \times 10^{-1}$

$\tilde{P}r_4 = 1$ $\beta_i = 1$

$\alpha_{2,1} = 4.26 \times 10^{1}$

$\alpha_{2,2} = 8.61 \times 10^{-1}$

$\alpha_{2,3} = -3.84 \times 10^{-1}$

$\gamma_1 = -1.72 \times 10^{-2}$ $\gamma_{1,1} = -3.85 \times 10^{-4}$

$\gamma_2 = 9.01 \times 10^{-2}$ $\gamma_{1,2} = 1.33 \times 10^{-2}$

$\gamma_3 = 1.16 \times 10^{-1}$ $\gamma_{1,3} = -1.29 \times 10^{-3}$

$\gamma_{2,1} = 2.41 \times 10^{-2}$

$\gamma_{2,2} = -2.65 \times 10^{-2}$

$\gamma_{2,3} = 2.44 \times 10^{-3}$

*Mixture No.* 4: 0.2 $N_2$+0.8 He (given in mass fractions)
Temperature 1034 K
Prandtl number of the mixture = 0.60995
Schmidt number: 1.4294

$$\text{matrix } \boldsymbol{\Omega} = \begin{bmatrix} 7.52 \times 10^{-1} & 1.73 \times 10^{-2} & -1.73 \times 10^{-2} \\ 2.87 \times 10^{0} & 1.59 \times 10^{0} & -5.92 \times 10^{-1} \\ 0 & 0 & 1 \end{bmatrix}$$

$\tilde{P}r_1 = 6.071 \times 10^{-1}$ $\alpha_{1,1} = 3.206 \times 10^{0}$

$\tilde{P}r_2 = 1.436 \times 10^{0}$ $\alpha_{2,1} = -5.193 \times 10^{1}$

$\tilde{P}r_3 = 1$ $\beta_i = 1$

$\gamma_1 = 9.419 \times 10^{-1}$ $\gamma_{1,1} = 1.814 \times 10^{-2}$

$\gamma_2 = 5.815 \times 10^{-2}$ $\gamma_{1,2} = -1.814 \times 10^{-2}$.